Geochemistry Geophysics Geosystems G3
AN ELECTRONIC JOURNAL OF THE EARTH SCIENCES
Published by AGU and the Geochemical Society

Article
Volume 4, Number 9
12 September 2003
8616, doi:10.1029/2001GC000215
ISSN: 1525-2027

A numerical model of hydrothermal cooling and crustal accretion at a fast spreading mid-ocean ridge

Abdellah S. M. Cherkaoui
School of Oceanography, University of Washington, Seattle, Washington 98195, USA (abdul@ocean.washington.edu)

Now at Earth Sciences Department, University of California, Santa Cruz, California 95064, USA

William S. D. Wilcock
School of Oceanography, University of Washington, Seattle, Washington 98195, USA (wilcock@ocean.washington.edu)

Robert A. Dunn
Department of Geology and Geophysics, University of Hawaii, Honolulu, Hawaii 96822, USA (dunn@emma.geo.brown.edu)

Douglas R. Toomey
Department of Geological Sciences, University of Oregon, Eugene, Oregon 97403, USA (drt@newberry.brown.edu)

[1] There are two competing models for lower crustal accretion at fast spreading ridges. In the gabbro glacier model, all the lower crust solidifies in a magma lens at the dike/gabbro boundary and then flows to its final level. In the sheeted sill model, the lower crust is formed by sills emplaced at a variety of depths. We present a steady state numerical representation of the sill model that explicitly includes hydrothermal circulation. The crust is accreted uniformly at the ridge axis at all depths and hydrothermal circulation occurs in crustal rocks that have cooled below a threshold temperature. The results show that when the permeability exceeds a threshold value ($\sim 4 \times 10^{-14}$ m^2 for a cracking temperature of 800°C and a uniform permeability), hydrothermal circulation can cool the entire crust near the ridge axis, producing vertical isotherms in the lower crust. At lower permeabilities, the properties of seawater lead to bimodal cooling with the lowermost crust cooling more slowly than shallower depths. These results are reasonably consistent with studies of the seismic structure of the East Pacific Rise and of plagioclase crystal size distributions in gabbros from Oman. We infer that the sheeted sill model cannot be discarded on thermal grounds.

Components: 7360 words, 11 figures.

Keywords: Mid-ocean ridge processes; hydrothermal cooling; numerical model; crustal accretion; fast-spreading ridge.

Index Terms: 3035 Marine Geology and Geophysics: Midocean ridge processes; 3230 Mathematical Geophysics: Numerical solutions; 3025 Marine Geology and Geophysics: Marine seismics (0935).

Received 15 August 2001; **Revised** 23 April 2003; **Accepted** 17 July 2003; **Published** 12 September 2003.

Cherkaoui, A. S. M., W. S. D. Wilcock, R. A. Dunn, and D. R. Toomey A numerical model of hydrothermal cooling and crustal accretion at a fast spreading mid-ocean ridge, *Geochem. Geophys. Geosyst.*, *4*(9), 8616, doi:10.1029/2001GC000215, 2003.

Theme: The Oman Ophiolite and Mid-Ocean Ridge Processes

1. Introduction

[2] Over the past decade, there has been a concerted effort to develop models of crustal accretion at fast spreading ridges that can explain seismic constraints from the East Pacific Rise and petrological and structural observations in the Oman ophiolite. This work has led to a variety of models for the formation of the lower crust that are defined by two end-members. The gabbro glacier or conveyor belt models [*Nicolas et al.*, 1988; *Henstock et al.*, 1993; *Nicolas et al.*, 1993; *Phipps Morgan and Chen*, 1993; *Quick and Denlinger*, 1993; *Phipps Morgan et al.*, 1994] are based on a idea first proposed by *Sleep* [1975]. The gabbros crystallize in a small magma lens at the dike/gabbro boundary and then subside to form the lower crust (Figure 1a). In the sheeted sill model [*Boudier et al.*, 1996; *Kelemen et al.*, 1997; *Kelemen and Aharonov*, 1998; *MacLeod and Yaouancq*, 2000], magma is fed through a series of thin sills at varying depths between the Moho and the dike/gabbro boundary and the lower crust crystallizes in situ (Figure 1b). Hybrid models combine varying proportions of gabbro flow and sill emplacement and/or include crystallization in a pair of magma lenses located at the dike/gabbro boundary and the Moho [*Schouten and Denham*, 1995; *Boudier et al.*, 1996; *Chenevez et al.*, 1998; *Chen*, 2001].

[3] One argument cited in support of the gabbro glacier model is that the strains generated by lower crustal flow match the vertical variations in the strength and dip of layering observed in the gabbros of the Oman ophiolite [*Phipps Morgan and Chen*, 1993; *Quick and Denlinger*, 1993]. Petrophysical studies of the gabbros find no evidence for plastic deformation of individual crystals but gabbro flow is still possible by lubricated grain boundary sliding and pressure solution if at least a few percent melt is present [*Nicolas*, 1992; *Nicolas and Ildefonse*, 1996].

[4] There are, however, several characteristics of the Oman ophiolite that are poorly explained by the gabbro glacier model. Short-wavelength correlated variations in mineral compositions in the lower gabbros appear inconsistent with melt transport by porous flow and thus with the melt fractions necessary for magmatic deformation [*Korenaga and Kelemen*, 1998]. Modal layering observed in the lower gabbros could not survive the large strains associated with ductile flow [*Boudier et al.*, 1996; *Kelemen et al.*, 1997]. There is a progressive decrease in plagioclase zoning down section in the gabbros that seems inconsistent with crystallization at a single location [*Pallister and Hopson*, 1981; *MacLeod and Yaouancq*, 2000]. Near-vertical fabric in the upper gabbros appears to be a primary feature that records melt flow rather than the accumulated strain [*MacLeod and Yaouancq*, 2000]. Cumulatively, these observations have led several recent studies to conclude that nearly all the lower crust crystallizes near the depth at which it is emplaced [*Kelemen and Aharonov*, 1998; *Korenaga and Kelemen*, 1998; *MacLeod and Yaouancq*, 2000].

[5] A second argument for the gabbro glacier model is that it provides the most physically consistent thermal model for lower crustal accretion. The heat of solidification is released in the axial magma lens where it can be extracted efficiently by axial hydrothermal systems. The effects of hydrothermal cooling have been included in numerical simulations by assuming an enhanced thermal conductivity at temperatures beneath a threshold cracking temperature [*Henstock et al.*, 1993; *Phipps Morgan and Chen*, 1993]. This effect is parameterized in terms of a "Nusselt number", a ratio of the total heat transported to that which would occur by conduction in the absence of hydrothermal circulation. If hydrothermal cooling transports about an order of magnitude more heat than conduction alone, the gabbro glacier model can match variations in the depth of a steady state axial magma chamber with spreading rate, including its absence along slow-spreading ridges [*Phipps Morgan and Chen*, 1993]. Most simulations predict that the hot ductile region underlying the axial magma chamber broadens progressively with depth through the lower crust (Figure 1a). Since the thermal gradients are small in this region, conductive cooling is inefficient and inconsistent with models in which more than about 10% of the lower crust

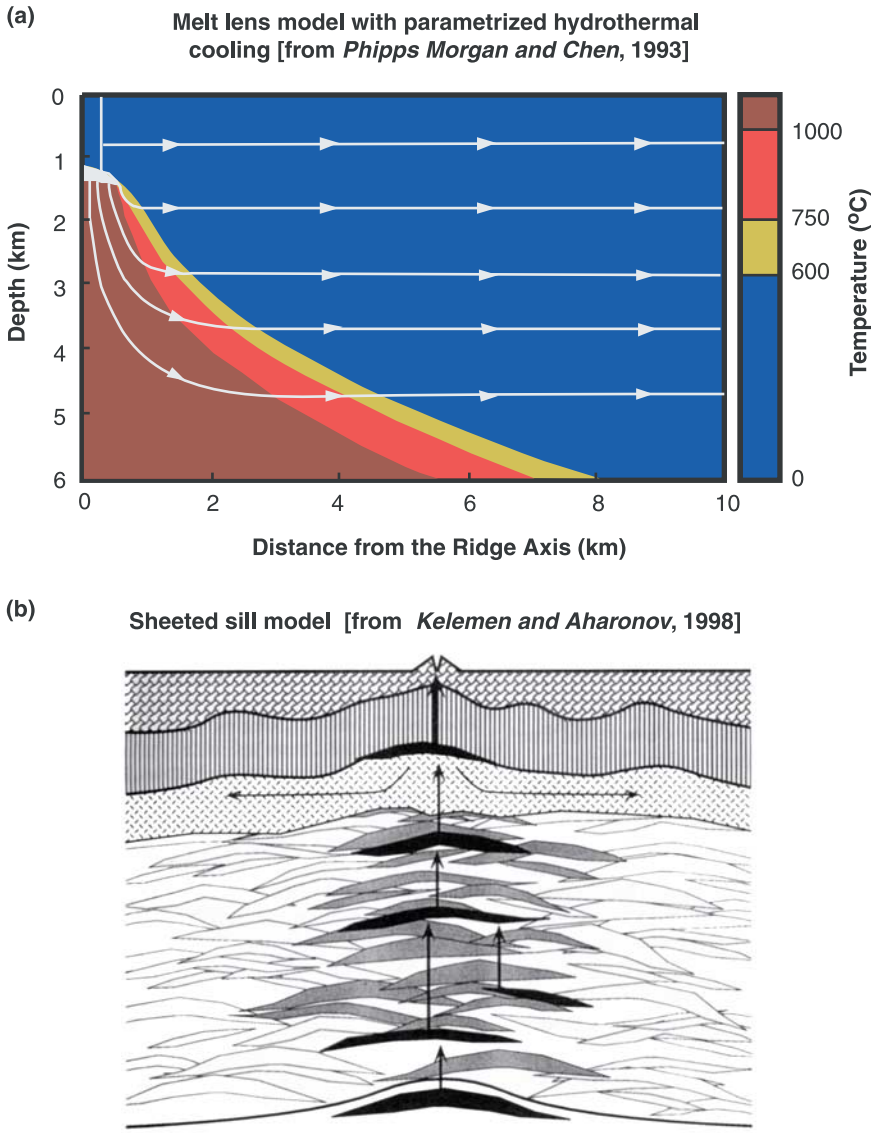

Figure 1. (a) Thermal structure and crustal flow streamlines derived by *Phipps Morgan and Chen* [1993] for a gabbro glacier model of crustal formation in which all the lower crust solidifies in a magma lens at the dike/gabbro boundary. The half-spreading rate is 50 mm/yr and hydrothermal circulation is parameterized by an eight-fold increase in thermal conductivity at temperatures below 600°C (based on Figure 4 of *Phipps Morgan and Chen* [1993]). (b) Schematic diagram showing the sheeted sill model (based on Figure 11c of *Kelemen and Aharonov* [1998]).

crystallizes well below the axial magma chamber [*Chen*, 2001].

[6] There is, however, good reason to question whether the "Nusselt number" parameterization is adequate for modeling the effects of hydrothermal circulation in crustal accretion. Conductive solutions have smooth gradients and uniformly distributed heat extraction, but these characteristics are unrealistic when considering the thermal structure at scales smaller than a single hydrothermal cell. Recent studies provide direct evidence that the thermal structure predicted by most parameterized simulations is incorrect. A tomographic study of the P wave velocity structure near 9°30′N on the East Pacific Rise [*Dunn et al.*, 2000] shows that the axial low velocity zone is steep sided and 5–7 km wide through most of the lower crust (Figure 2). Similarly, models of S-wave velocity obtained

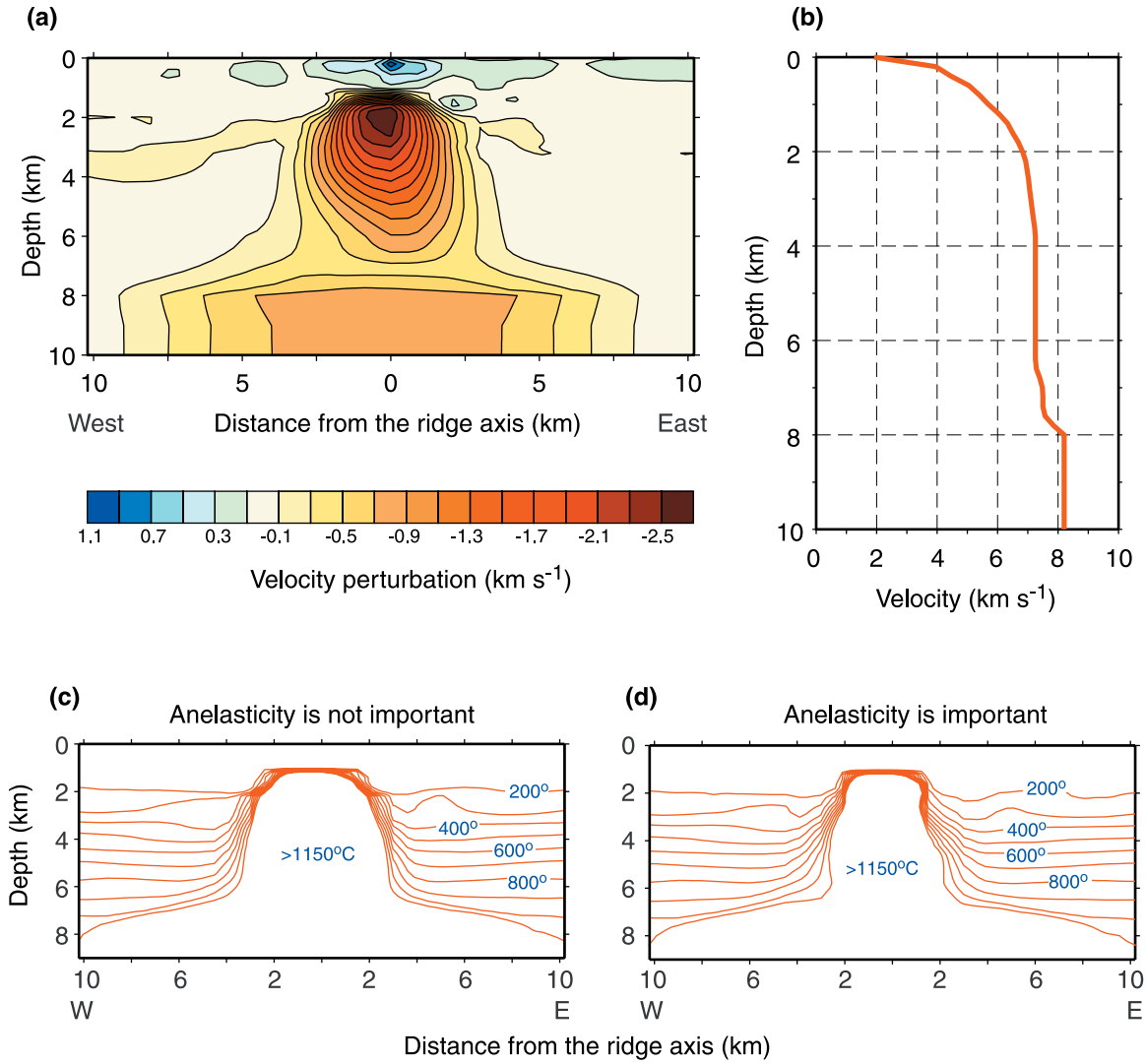

Figure 2. Velocity structure for a two-dimensional tomographic inversion on the East Pacific Rise at 9°30′N and inferred temperatures (from *Dunn et al.* [2000]). Both (a) the velocity perturbations and (b) the one-dimensional reference velocity model are shown. The basic features of the velocity perturbation model are not strongly sensitive to the assumed crustal thickness. Models of the thermal structure were derived from the inversions assuming (c) anharmonic effects only and (d) both anharmonic and anelastic effects. These represent approximate minimum and maximum estimates of the contribution of temperature to the low velocity zone [*Dunn et al.*, 2000]. Note that these thermal models assume a reference structure well off-axis with uniform vertical gradients, but that this is not required by the seismic data.

from seafloor compliance measurements at 9°33′N and 9°48′N on the East Pacific Rise [*Crawford and Webb*, 2002] indicate that the axial partial melt zone is less than 8 km wide throughout the crust. An analysis of plagioclase crystal size distributions in gabbros from Oman [*Garrido et al.*, 2001] shows that the cooling rates do not increase smoothly with depth but have a bimodal distribution with markedly slower cooling rates in the lowermost crust. In the upper half of the plutonic section, the cooling rates are consistent with closely spaced steep isotherms located within a few kilometers of the ridge.

[7] In this paper we present a simple steady state model for the accretion and hydrothermal circulation in the oceanic crust in which melt crystallizes at its final depth of emplacement. The results predict thermal structures that are reasonably consistent with the recent observations. We argue that

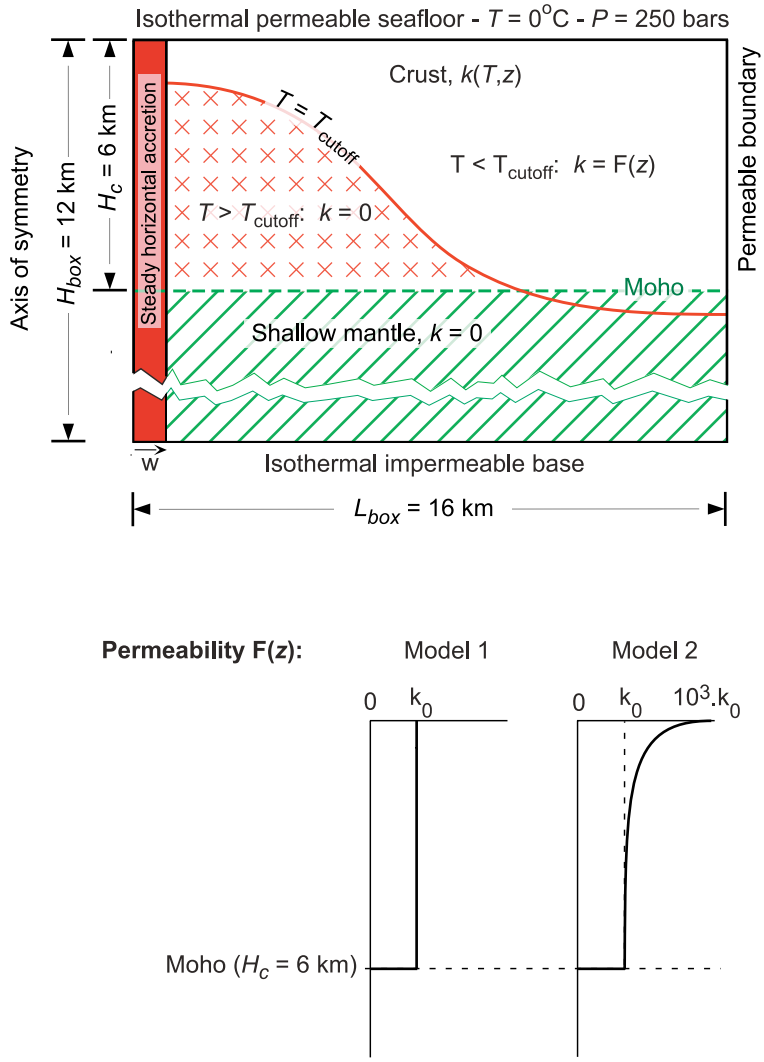

Figure 3. Configuration of the numerical model. Solutions are presented for both uniform and temperature- and pressure-dependent fluid properties and for two permeability structures.

the sheeted sill model cannot be rejected on thermal grounds.

2. Model

[8] Our two-dimensional numerical model (Figure 3) measures 16 km × 12 km. The upper left-hand corner is the ridge axis and the crust is 6 km thick. For simplicity, we ignore vertical flow of melt and convection in melt bodies; new lithosphere accretes continuously along the left-hand boundary and all lithic material advects to the right at a half-spreading rate of 50 mm/yr. The accreted crust is molten and at the liquidus temperature. Since we are interested primarily in the accretion of the lower crust we use a temperature-dependent latent heat of crystallization for a bulk composition obtained for a lower crustal section in Wadi Khafifah (Kelemen and Garrido, unpublished data) in the Oman ophiolite derived with the MELTS software [*Ghiorso*, 1997]. Crystallization begins at the liquidus temperature of 1248°C with 50% solidification completed at 1229°C, 90% at 1100°C and 100% at 1000°C. The calculated average latent heat of solidification is 384 kJ/kg. We assume a heat capacity of 1.2 kJ kg^{-1} $°C^{-1}$ and a thermal conductivity that decreases non-linearly from 2.5 W m^{-1} $°C^{-1}$ at 0°C to nearly 1.4 W m^{-1} $°C^{-1}$ at 1248°C [*Clauser and Huenges*, 1995]. For a crustal den-

sity of 2800 kg/m^3, the thermal diffusivity of the crust at 0°C is 7.4 × 10^{-7} m^2 s^{-1}.

[9] The top boundary of the model is permeable, isobaric (250 bars) and isothermal (0°C). Following earlier models [*Morton and Sleep*, 1985; *Phipps Morgan and Chen*, 1993], we assume that the crustal rocks are impermeable above a threshold "cracking" temperature. Below this temperature, we assume the crust is a porous continuum in which fluid flow obeys Darcy's Law. The mantle is impermeable at all temperatures, an assumption that is consistent with conceptual models that suggest hydrothermal circulation is sluggish in the mantle [*Wilcock and Delaney*, 1997]. For simplicity and because our knowledge of the permeability of young oceanic crust is limited, we consider only two permeability distributions in the cracked medium (Figure 3). One is uniform, while in the other the permeability decreases exponentially by three orders of magnitude between the seafloor and the base of the crust. The model dimensions were chosen such that the right-hand and bottom boundaries have a negligible effect on the crustal thermal structure near the rise axis.

[10] We approximate the thermodynamic properties of the hydrothermal fluid with a 3.2 weight-percent NaCl solution [*Bischoff and Rosenbauer*, 1985] using an experimentally determined equation of state [*Pitzer et al.*, 1984; *Anderko and Pitzer*, 1993]. The fluid viscosity comes from a formula for pure water [*Meyer et al.*, 1993]. We consider only one-phase porous flow; in the two-phase region we use the thermodynamic properties of the two-phase mixture and the viscosity of the dominant phase [*Wilcock*, 1998].

[11] To solve for hydrothermal flow and temperature, we non-dimensionalize the appropriate equations of conservation of mass, energy and momentum [*Cherkaoui et al.*, 1997; *Wilcock*, 1998] and obtain numerical solutions using a finite-volume formulation [*Patankar*, 1980]. At the start of each time step, material is emplaced at the ridge axis and the domain is advected horizontally over a distance equal to the width of rock emplaced. A solution for temperature and hydrothermal flow at the end of the time step is then obtained iteratively. We performed numerical experiments with grid refinement and scale analysis to establish the optimal spatial and temporal discretization. We present solutions with permeabilities up to 7 × 10^{-14} m^2 for a mesh of 160 x 80 control volumes. The grid spacing is 100 m in the horizontal direction and increases non-uniformly downward from nearly 3 m at the seafloor to 50 m at the base of the model. With a time step of 4000 years, a steady state is typically reached in 250,000–550,000 years.

3. Results

[12] Our model differs from the gabbro glacier simulations [*Henstock et al.*, 1993; *Phipps Morgan and Chen*, 1993], both in the style of magmatic accretion and because we explicitly incorporate hydrothermal circulation. In order to assess the effect of changing just the pattern of accretion, we first calculated a conductive solution (Figure 4) with a "Nusselt number" parameterization mimicking that of Figure 1a. Following *Phipps Morgan and Chen* [1993], the thermal conductivity is 3.36 W m^{-1} °C^{-1} (equivalent to a thermal diffusivity of 10^{-6} m^2) at high-temperature and increases eight-fold below 600°C. The dimensions of the hot, impermeable region in our solution are similar to the corresponding gabbro glacier simulation of Figure 1a, but because the melt solidifies at its final depth of emplacement, our solution includes a large region of molten crust.

[13] We present four sets of solutions with hydrothermal flow, each of which comprises simulations for a range of reference permeabilities. The first two sets (Figures 5 and 6) were calculated assuming uniform fluid properties and permeability, and cracking temperatures of 600°C and 800°C, respectively. Although the fluid properties are unrealistic, the solutions illustrate the basic patterns of convective cooling and serve as a useful reference for comparison with more complex models. For each solution in Figures 5 and 6, we show the temperature structure in the left panel and the Darcy velocity in the right panel. We cannot calculate a "Nusselt number" from our solutions that can be meaningfully compared with those obtained from conductive models [*Henstock et al.*, 1993; *Phipps Morgan*

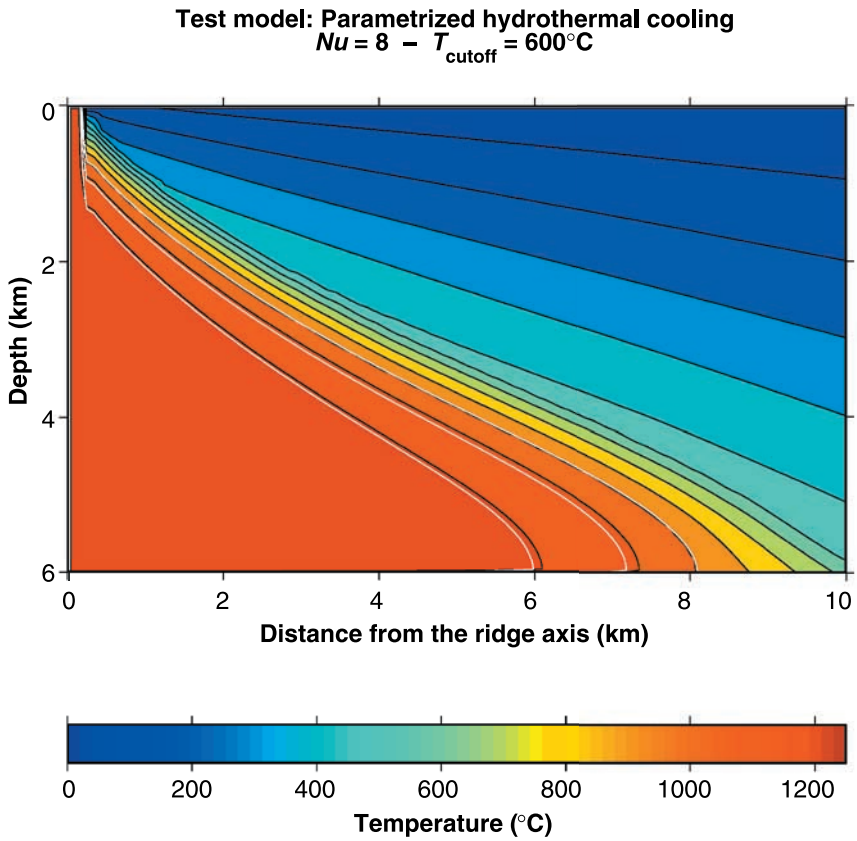

Figure 4. Thermal structure predicted for a simulation in which hydrothermal circulation is parameterized by an eightfold increase in an otherwise constant thermal conductivity at temperatures less than 600°C. White contour lines represent 0%, 50% and 100% melt.

and Chen, 1993]. In our solutions the relative importance of convective heat transport varies with distance from the ridge axis. A "Nusselt number" obtained for the whole model domain would be essentially constant for all solutions that cool the entire crust since they transport the same amount of heat. To characterize the convective vigor of each simulation, we calculated the ratio of the integrated advective and conductive heat fluxes across a plane just below the seafloor (Figure 7).

[14] The primary feature of the solutions is that as the permeability increases, the width of the hot, impermeable region decreases and the dip of its boundary steepens. At permeabilities, k_0 of $\sim 10^{-15}$ m^2 and below (Figures 5a–5b and 6a–6b), hydrothermal cooling is inefficient, heat transport is dominated by conduction (Figure 7), and the solutions predict a very large lower crustal magma chamber. Once the permeability increases above about 2×10^{-15} m^2, heat transport is convection dominated and the solutions enter a regime where they are sensitive to permeability. For a cracking temperature of 600°C, the half-width of the impermeable zone at the base of the crust decreases from >12 km at a $k_0 = 7 \times 10^{-15}$ m^2 (Figure 5c) to under 6 km at $k_0 = 7 \times 10^{-14}$ m^2 (Figure 5f). For the higher cracking temperature of 800°C, the half-width decreases more rapidly from about 8 km at $k_0 = 7 \times 10^{-15}$ m^2 (Figure 6c) to 3 km at $k_0 = 2 \times 10^{-14}$ m^2 (Figure 6d). At permeabilities of $k_0 = 4 \times 10^{-14}$ m^2 and above (Figures 6e–6f), hydrothermal circulation extracts all the magmatic heat at the ridge axis and the impermeable region has a near-vertical boundary and a half width of less than 1 km. Our numerical discretization is inadequate to resolve solutions at permeabilities much above 7×10^{-14} m^2 but we infer that at higher permeabilities solutions with the 600°C cracking temperature would evolve to solutions similar to Figures 6e–6f.

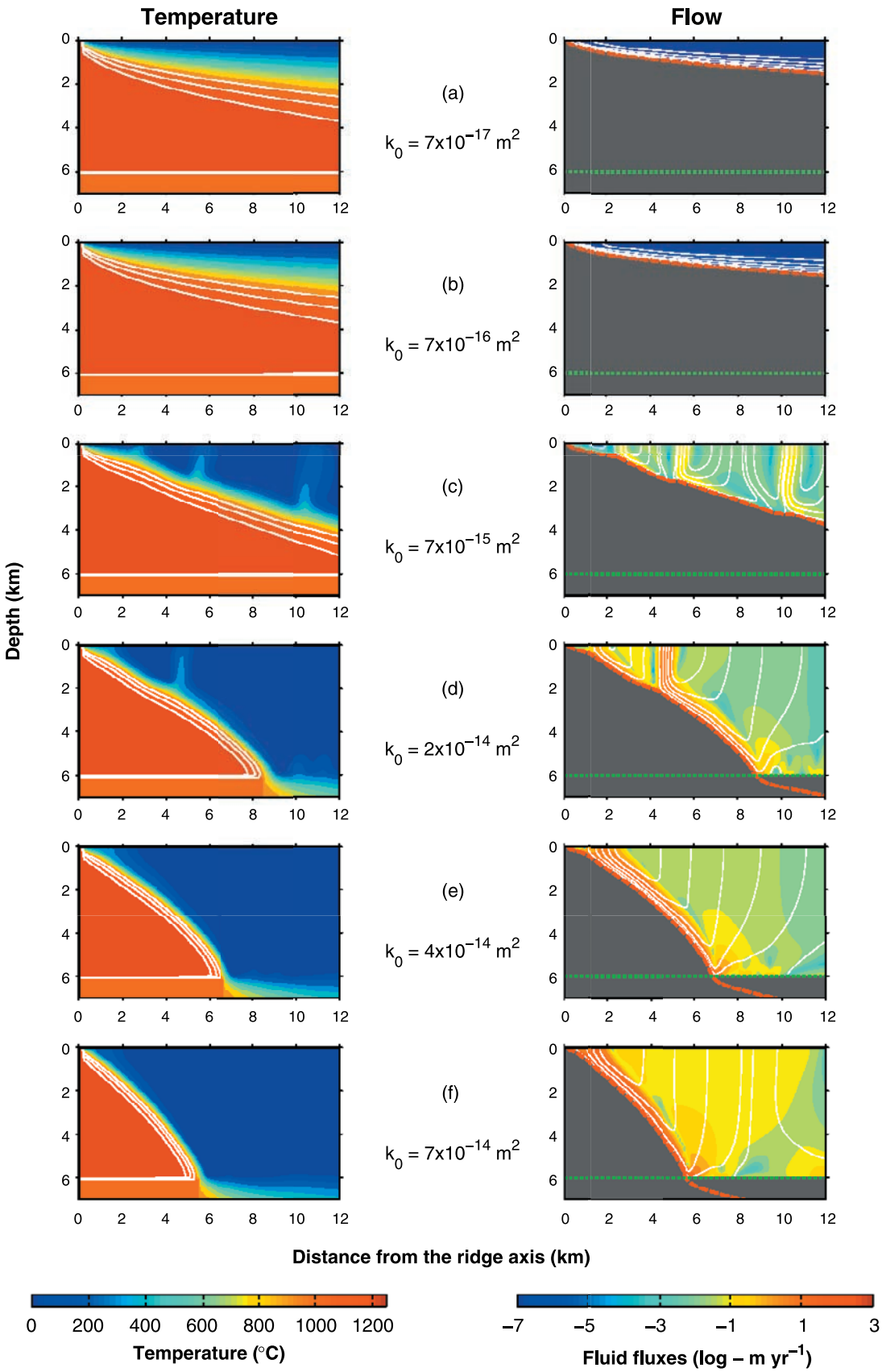
Temperature
Flow
(a)
$k_0 = 7x10^{-17}$ m^2
(b)
$k_0 = 7x10^{-16}$ m^2
(c)
$k_0 = 7x10^{-15}$ m^2
(d)
$k_0 = 2x10^{-14}$ m^2
(e)
$k_0 = 4x10^{-14}$ m^2
(f)
$k_0 = 7x10^{-14}$ m^2
Depth (km)
Distance from the ridge axis (km)
0 200 400 600 800 1000 1200
Temperature (°C)
−7 −5 −3 −1 1 3
Fluid fluxes (log – m yr^{-1})

[15] Our solutions are characterized by hydrothermal cells that flow up the impermeable boundary. Earlier work has shown that a sloping lower boundary stabilizes wide cells [*Rabinowicz et al.*, 1999], and these effects are apparent in our solutions. In Figures 5c–5d and 6c the hot crustal zone is cooled by more than one cell and regions of hydrothermal upflow develop off axis. The solutions generally achieve a steady state because these cells migrate toward the ridge axis at the spreading rate, although in some instances the cells oscillate back and forth. For solutions in which the hot impermeable zone has a half width of less than 8 km at the base of the crust (Figures 5e–5f and 6d–6f), the crustal magma is cooled by a single cell that vents at the ridge axis. Unsteady flow is a common characteristic of high Rayleigh number convective solutions with bottom heating [*Cherkaoui and Wilcock*, 1999, 2001]. While it has been shown that a sloping lower boundary inhibits unsteadiness [*Rabinowicz et al.*, 1999] and that unsteady flow does not occur for heating from the side [*Gill*, 1969], it is possible that our discretization is too coarse to resolve fine-scale unsteady flow at higher permeabilities. In this case our steady state solutions may slightly underestimate the hydrothermal heat transport and thus, overestimate the width of the impermeable region for a given permeability.

[16] The third set of solutions (Figure 8) are for a cracking temperature of 800°C but unlike Figure 6 include temperature- and pressure-dependent fluid properties. At the lowest and highest permeabilities shown the large-scale thermal structure is very similar to that obtained with uniform fluid properties, but the intermediate solutions are significantly different and show a bimodal pattern of cooling. At $k_0 = 7 \times 10^{-15}$ m^2 and 2×10^{-14} m^2 (Figures 8c–8d), the boundary of the hot, impermeable region is characterized by a decrease in slope below about 3 km depth and the hydrothermal upflow velocities are much higher in the upper part of the crust. At $k_0 = 2 \times 10^{-14}$ m^2, the half-width of the impermeable zone is only 2 km at a depth of 3 km but at the base of the crust it extends to the edge of the model (>12 km).

[17] The effects of non-uniform fluid properties can be considered in terms of the fluxibility [*Lister*, 1995; *Jupp and Schultz*, 2000], which measures the ability of hydrothermal flow to transport energy and is given by:

$$F = \frac{\left(\rho_{f\,0} - \rho_f\right)\rho_f H}{\mu} \qquad (1)$$

where ρ_f is the fluid density, ρ_{f0} is the cold fluid density, H is the fluid enthalpy relative to the cold fluid and μ is the viscosity. At a given pressure, the maximum fluxibility (Figure 9a) occurs at temperatures just above the two-phase curve. *Jupp and Schultz* [2000] argue that plumes will form preferentially where $|\partial F/\partial T|$ is a maximum. For a given pressure, the maximum $|\partial F/\partial T|$ value (Figure 9b) occurs at a temperature just below the two-phase curve and this maximum decreases substantially with increasing pressure. As the permeability increases one would expect vigorous upwelling to develop first at shallower depths where $|\partial F/\partial T|$ is highest and this may explain why the lower half of the crust cools comparatively slowly in the solutions of Figures 8c–8d.

[18] The fourth set of solutions (Figure 10) are the same as the third except that the permeability

Figure 5. (opposite) Six solutions for a model with uniform fluid properties and uniform crustal permeability below a cracking temperature of 600°C. The relative values of the permeability are determined by the Rayleigh number and the absolute values have been chosen so that the heat transport characteristics of the solutions approximately match the solutions for variable properties (see Figure 7). The permeabilities shown are a factor of 15 less than those obtained from the Rayleigh number assuming cold water properties (density, $\rho = 1035$ kg m^{-3}; volumetric coefficient of thermal expansion, $\alpha = 10^{-4}$ °C^{-1}; heat capacity, $c_p = 4.2$ kJ °C^{-1} kg^{-1}; and viscosity, $\mu = 1.4 \times 10^{-3}$ Pa s). For each solution, the left-hand panel shows the thermal structure as shaded contours. White contours delineate boundaries of 100%, 50%, and 0% melt (i.e., temperatures of 1248°C, 1229°C and 1100°C). The right-hand panel shows the flow speed (shaded contours) and direction (white streamlines) of hydrothermal circulation. Black regions are impermeable. Note that Darcy velocities are generally much higher near the spreading axis. The Moho (green dotted line) and 600°C cracking isotherm (red dashed line) are also shown. All the solutions are plotted at the beginning of a time step.

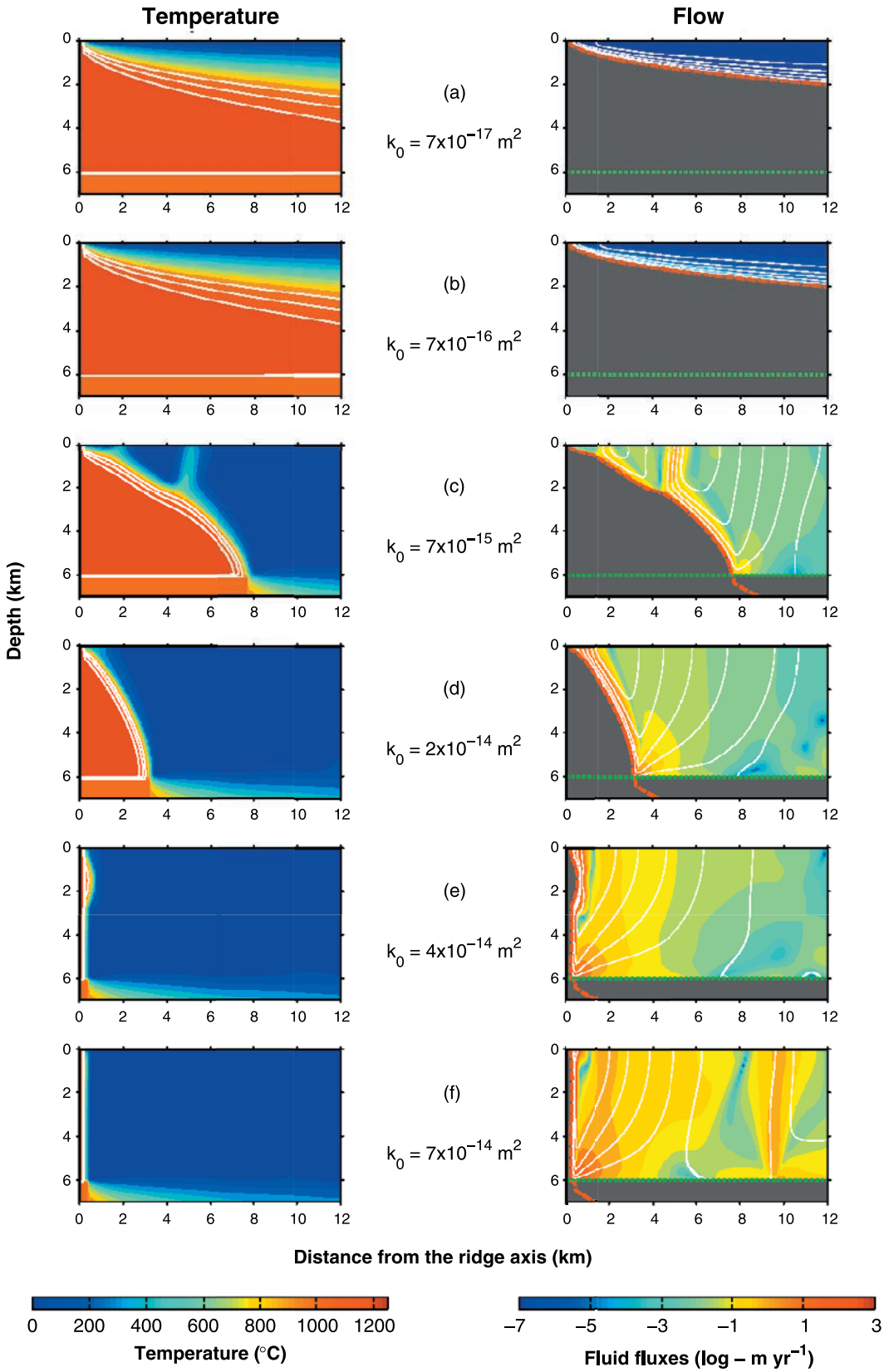

Figure 6. As for Figure 5 except that the cracking temperature is 800°C.

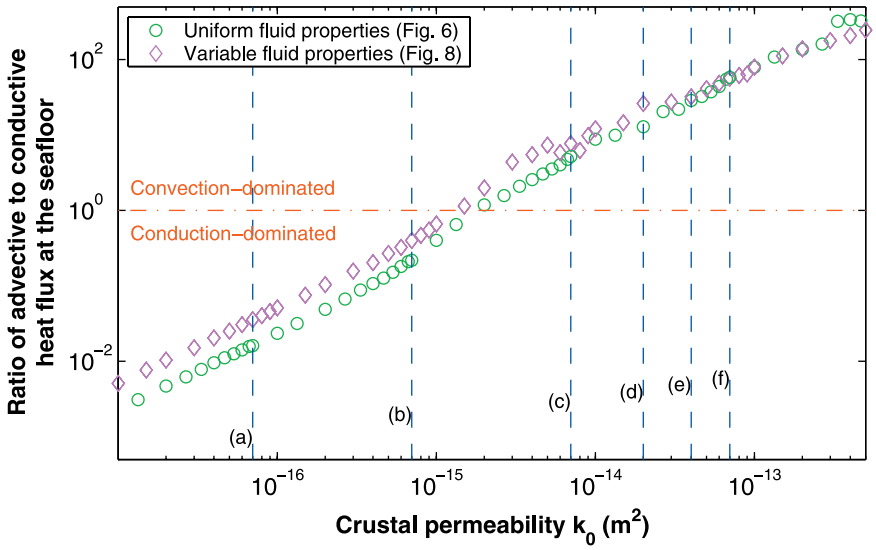

Figure 7. Ratio of advective to conductive heat flux crossing a horizontal boundary just below the seafloor for the models with a cracking temperature of 800°C, uniform permeability and either uniform (green circles) or variable (purple diamonds). Vertical dashed lines show the permeabilities for the solutions plotted in Figures 5, 6, 8, and 10.

decreases by three orders of magnitude down through the crust (Model 2 in Figure 3). These solutions show a progression that is very similar to Figure 8. Since the permeability is higher at shallow depths in these models (Figure 3), hydrothermal cooling is more efficient for a given k_0 and solutions with a narrow hot, impermeable region develop at a lower k_0.

4. Discussion

[19] In this paper, we have presented numerical simulations for a steady state thermal model of crustal formation at a fast spreading ridge. Melt accretes uniformly in a dike-like structure beneath the spreading axis and the model explicitly includes hydrothermal circulation in crust that has cooled below a 'cracking' temperature. The results show that for permeabilities exceeding a threshold value ($\sim 4 \times 10^{-14}$ m^2 for a uniform permeability model with a cracking temperature of 800°C), hydrothermal circulation cools the entire crust efficiently and leads to near-vertical isotherms in the lower crust. At slightly lower permeabilities, the properties of seawater can lead to bimodal cooling with the lowermost crust cooling significantly more slowly than at shallower depths.

[20] Seismic results from the East Pacific Rise show that a thin axial magma lens at 1–2 km depth [*Detrick et al.*, 1987] is underlain by a steep-sided low velocity zone that is less than 8 km wide [*Dunn et al.*, 2000; *Crawford and Webb*, 2002] and contains relatively low melt fractions [*Wilcock et al.*, 1992; *Dunn et al.*, 2000]. Our models can reproduce the steep sides of the crustal low-velocity zone but cannot reproduce both its width and melt content. Solutions with an impermeable region that is sufficiently wide also include a lot of melt. Assuming the sheeted sill model, this discrepancy can be explained, at least partially, in terms of the width of accretion. In our simulations, all the crust accretes at the spreading axis while in the sheeted sill models melt is injected over a finite region whose width is presumably similar to that of the low velocity zone.

[21] Recent work in the Oman ophiolite suggests that cooling rates in the gabbros are bimodal and are about 1.5–2 times slower in the lowermost 2 km of crust [*Garrido et al.*, 2001]. The width of the low velocity zone (Figure 2) in the tomographic images also triples at the Moho [*Dunn et al.*, 2000]. Although the fine-scale velocity structure of the lowermost crust may not be well resolved by tomography, a boundary layer with

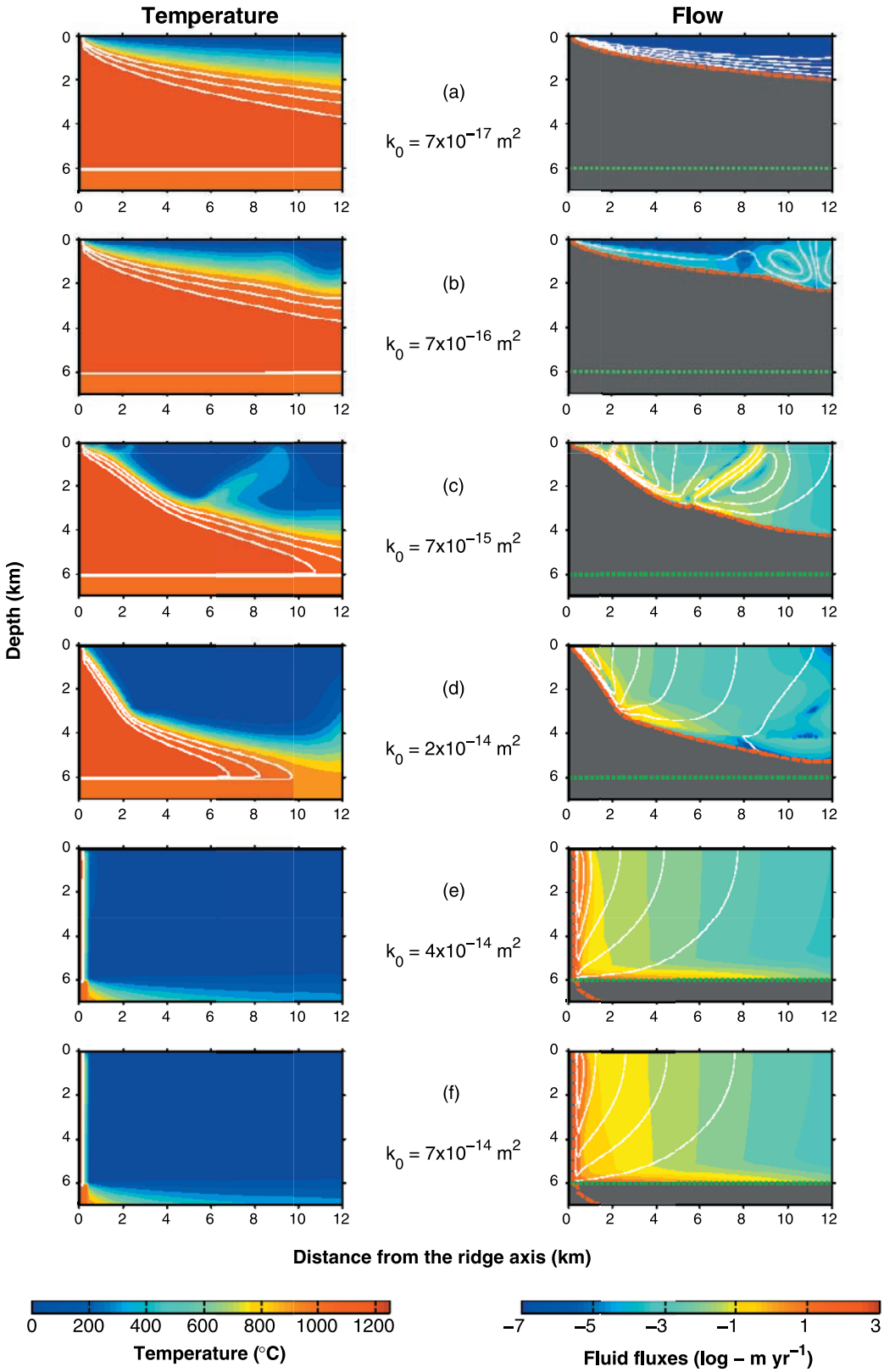

Figure 8. As for Figure 6 except the model includes temperature- and pressure-dependent fluid properties for a 3.2 wt% NaCl solution.

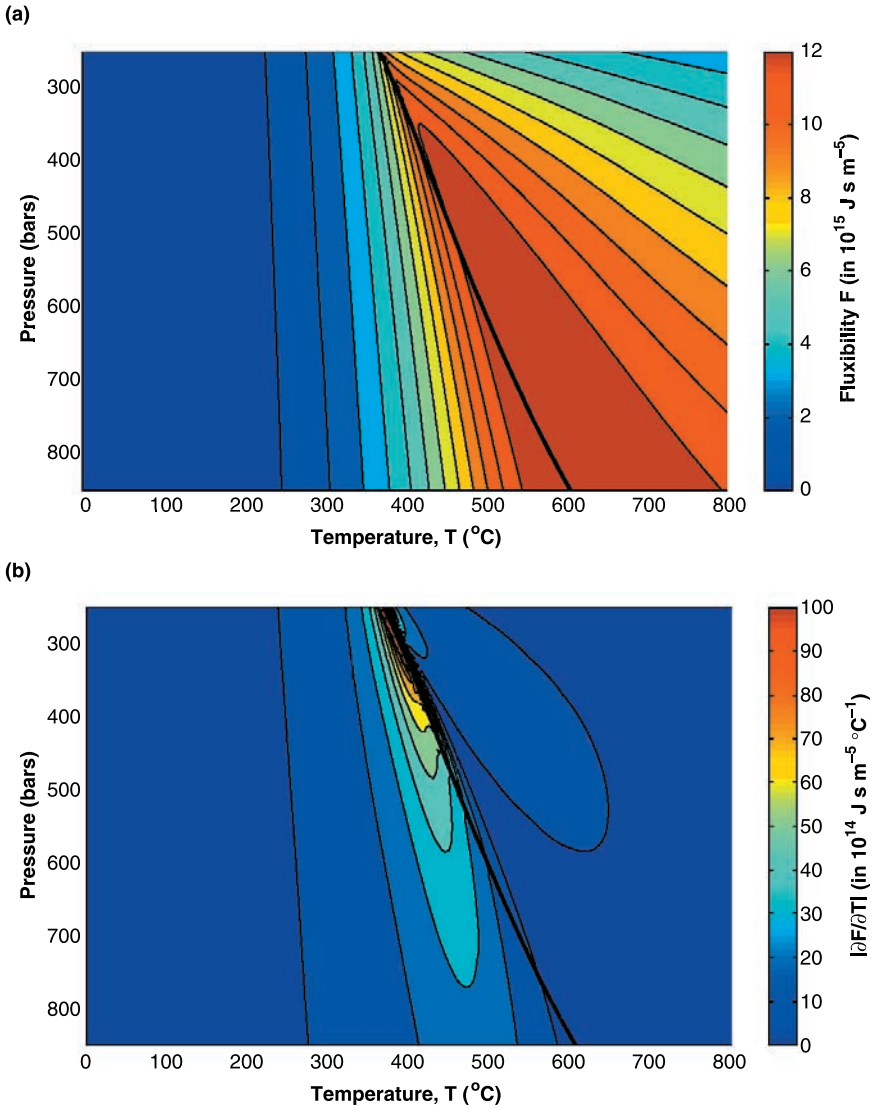

Figure 9. Contour plots of (a) the Fluxibility, F and (b) the magnitude of the fluxibility gradient $|\partial F/\partial T|$ for a 3.2 wt% NaCl solution derived using the equation of state of *Pitzer et al.* [1984] and *Anderko and Pitzer* [1993] and a fluid viscosity obtained from a formula for pure water [*Meyer et al.*, 1993].

a thickness of ~2 km must be present to insulate the hot, melt-rich region beneath the Moho. The slower cooling of the lowermost crust could result from a decreased permeability due to overburden pressure but our solutions also suggest that non-uniform fluid properties can produce bimodal cooling.

[22] In order to include hydrothermal circulation explicitly, our models are necessarily simplified and there are a number of underlying assumptions and features of the solutions that warrant further discussion. There is good geochemical evidence to support our key assumption that high-temperature fluid circulation exists in the lower crust. For instance, oxygen isotope ratios in the Oman ophiolite indicate pervasive circulation at temperatures above at least 400–500°C in the upper three-quarters of the crust and fluids reach the Moho locally [*Gregory and Taylor*, 1981] and metamorphic studies of gabbros from the East Pacific Rise [*Manning et al.*, 1996; *Manning and MacLeod*, 1996] and the Oman ophiolite [*Manning et al.*, 2001] document water penetration at temperatures

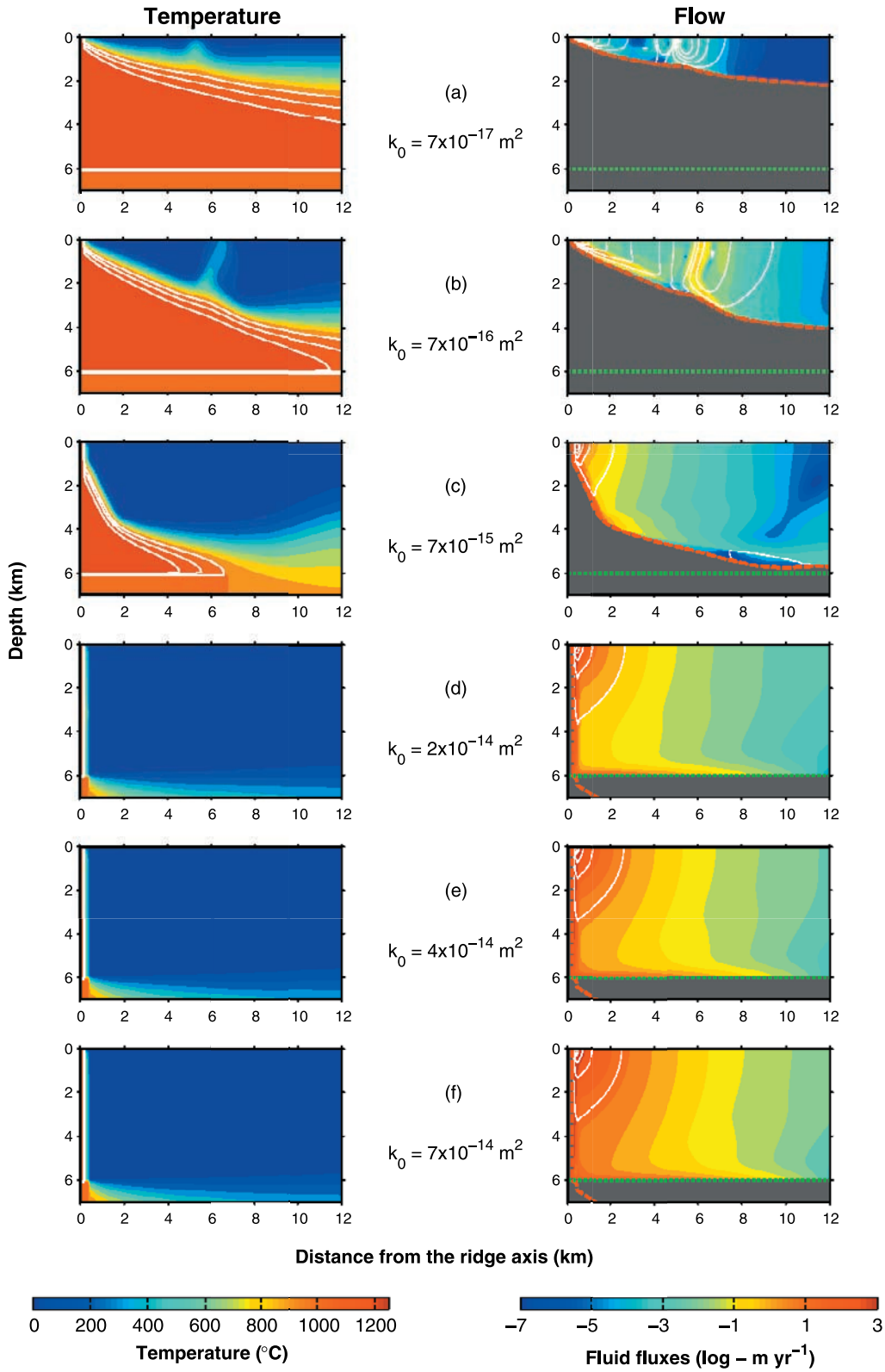

Figure 10. As for Figure 6 except the model includes temperature and pressure dependent fluid properties for a 3.2 wt% NaCl solution and a permeability that decreases exponentially by three orders of magnitude with depth (see Model 2 in Figure 3). The reference permeability shown is the permeability at the Moho.

of ~700–800°C. Thermodynamic models suggest that large volumes of fluid may circulate through the lower crust at temperatures above ~700°C [*McCollom and Shock*, 1998] without affecting the mineralogy. However most geochemists conclude that only a small volume of high-temperature fluids are involved and infer that this fluid either plays an insignificant role in heat transport through the lower crust or recirculates in a cell that is separated from hydrothermal flow in the upper crust [e.g., *Coogan et al.*, 2002].

[23] Geochemists quantify the relative volume of fluid involved in a hydrothermal reaction in terms of the water-rock ratio which is defined for batch laboratory experiments as the mass of seawater initially present in a reaction chamber divided by the mass of rock. For natural systems, the mass of water present at any particular instant is small fraction of the rock, but a meaningful water-rock ratio may be defined as the total mass of seawater which has passed through the system divided by the total mass of altered rock [*Mottl*, 1983]. For our numerical solutions we can calculate a water-rock ratio, Φ for the crustal reactions that occur near the ridge axis above a selected temperature T_S and below a particular depth horizon, h by:

$$\Phi = \frac{\int_0^{L_{cell}} \Gamma \rho_f |q(x,h)| dx}{\rho_r v (H_{crack} - h)} \quad (2)$$

where L_{cell} is the width of the axial cell, ρ_f and ρ_r are the fluid and rock density, q the Darcy velocity at the specified coordinates, v is the half spreading rate, H_{crack} the maximum depth of circulation of the axial cell, and $\Gamma = 1$ for $T \geq T_S$ and $q < 0$ (upward flow) and $\Gamma = 0$ otherwise. In Figure 11, we show calculated water-rock ratios as a function of temperature for circulation below 2 km (i.e. within the gabbros) for the solutions of Figures 8d–8e. The detailed characteristics of these curves are poorly resolved because the upflow is confined to a narrow region that is only a few cells wide but they indicate water-rock ratios of ~0.5 and ~1 at temperatures greater than 600°C and 400°C, respectively. The reason our models have water-rock ratios near or just below unity is that the heat capacity of water is high. The enthalpy of molten rock in our model relative to 0°C (1.9 x 10^3 kJ/kg) is similar to seawater at 550 bars and 400°C (1.7 x 10^3 kJ/kg) and significantly less than seawater at 550 bars and 600°C (2.9 $\times$ 10^3 kJ/kg) [*Anderko and Pitzer*, 1993].

[24] On the basis of oxygen isotope data, *Gregory and Taylor* [1981] estimate a water-rock ratio of 0.3–1 for the gabbros of the Oman ophiolite. At Hess Deep, *Lécuyer and Reynard* [1996] estimate water rock ratios of 0.1–0.5 and 0.2–1 from strontium and oxygen isotopes, respectively, and infer that the latter values are more reliable. While these values are typically interpreted otherwise, our results suggest that at least the higher values are consistent with circulation in a single layer open system. Furthermore, if hydrothermal flow is channelized, there may be a tendency for geochemical studies to underestimate average water-rock because of a sampling bias toward the freshest outcrops and away from the most altered and deformed regions.

[25] Our numerical solutions are based on the assumption that hydrothermal flow in the two-phase regime can be represented by a single-phase algorithm in which the thermodynamic properties are an average for the two-phase mixture. This may be reasonable if the small droplets of dense brine that condense during phase separation at supercritical pressures get swept along with the flow. However, *Bischoff and Rosenbauer* [1989] argue that supercritical two-phase separation will lead to the development of a stable two-layer pattern of convection in which an upper seawater cell overlies a recirculating brine cell with salinities ~10× seawater. Although this conceptual model is widely accepted, there is no conclusive evidence for such a configuration. Brines with such high salinities are too dense to vent at the seafloor and the briny fluid inclusions sampled in oceanic gabbros may be magmatic in origin [*Kelley and Frueh-Green*, 2001]. Clearly this is an unresolved issue that warrants further study although it would be computationally very challenging to repeat our models with a two-phase algorithm.

[26] Our models suggest that a permeability of at least ~4 $\times$ 10^{-14} m^2 is needed to cool the lower crust near the ridge axes. This value may be an

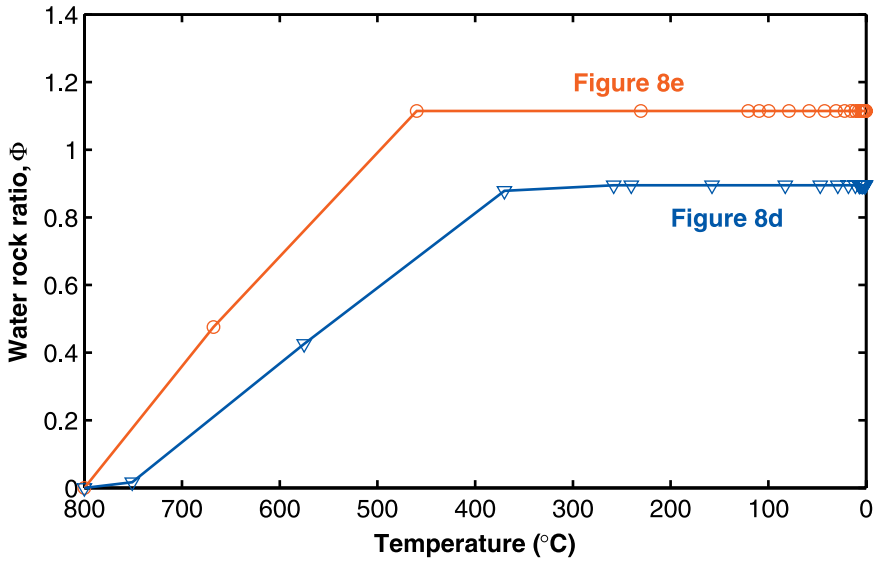

Figure 11. Fluid-rock ratios as a function of temperature calculated with equation (2) for the circulation beneath 2 km (i.e., the lower crust) for the solutions shown in Figures 8d and 8e. The curves show the mass flux of water that circulates out of the lower crust at or above a given temperature divided by the mass flux of new crustal rock added by ridge extension.

overestimate if our models fail to resolve all unsteady flow in the basal thermal boundary layer [*Cherkaoui and Wilcock*, 1999]. Alternatively, it may be an underestimate if convection occurs in a thermally less efficient two-layer system. It is clear that the required permeability is several orders of magnitude higher than the values of $\sim 10^{-17}$ m^2 typically measured or inferred for the middle and lower crust off axis [*Fisher*, 1998]. In the upper crust, flow channeling can lead to large scale permeabilities that are several orders of magnitude than typical borehole measurements [*Fisher and Becker*, 2000]. There are no direct constraints on the temporal evolution of permeability of the lower crust near mid-ocean ridges and it is conceivable that it may be temporarily high while the crust is undergoing rapid cooling and contraction. Indeed, we would argue that our modeling coupled with the seismic data from the East Pacific Rise provides an indirect constraint on the large scale permeability of young oceanic lower crust.

[27] Another feature of our models is that impermeable zones with a half-width matching the seismic observations contain a large fully molten region (e.g., Figure 9d). Conduction is inefficient over large distances (>$\sim$1 km at the timescale of interest) and for our simple model, melt that is injected near the center of an impermeable region will not solidify until it advects near the permeable zone. *Chen* [2001] concludes that such considerations can be used to invalidate the sheeted sill model but we would argue otherwise. Our models are greatly simplified and do not include melt migration, a depth-dependent composition and convection within melt bodies. We know that the lower crust is composed of cumulates which formed from partial crystallization of the melts that then rise to form the lower crust [*Pallister and Hopson*, 1981]. One consequence of this is that rather than being isothermal and fully molten as in our solutions, the lower crust may be both largely solid and include significant temperature gradients that can contribute to conductive heat loss [*Sinton and Detrick*, 1992]. If the sills in the sheeted sill model are preferentially injected near the margins of the impermeable zone or if they are able to transport heat convectively toward the margins, then the hydrothermal systems will be able to extract the latent heat of crystallization without requiring conduction over length scales of several kilometers. Our models are steady state but unsteady patterns of hydrothermal circulation may improve the efficiency of heat loss. We know that

hydrothermal venting is very unevenly distributed along ridges [*Haymon et al.*, 1991] and that diking-eruptive events drive spectacular bursts of hydrothermal activity [*Delaney et al.*, 1998]. We would argue that sill emplacement may have the same effect on circulation in the lower crust. It seems likely that the boundaries of hydrothermal circulation will move back and forth in response to magmatic fluctuations. Fluids may locally penetrate the low velocity zone near newly emplaced sills, leading to a very irregular boundary. *McCollum and Shock* [1998] question whether the boundary of hydrothermal flow can be equated to the brittle-ductile boundary. Thus the concept of a cracking front separating hydrostatic fluids from impermeable dry rock may not be applicable in the lower crust.

[28] Our model contrasts with earlier work in which hydrothermal cooling is parameterized by enhanced conductivity [*Henstock et al.*, 1993; *Phipps Morgan and Chen*, 1993]. These models predict isotherms that slope away from the ridge axis at modest dips. In a recent paper, *Chen* [2001] presents new solutions for the gabbro glacier model that have steep isotherms in the lower crust (see his Figure 2). This thermal structure is the result of incorporating a non-linear power law rheology (J. Chen, personal communication, 2001). It is important to point out that neither our models nor the seismic observations on the East Pacific Rise contradict the gabbro glacier model. Indeed, the gabbro glacier model provides an elegant explanation for the depth of the axial magma chamber and for the low melt content of the lower crustal low velocity zone [*Chen*, 2001]. However, we would argue that both gabbro glacier and sheeted sill models are thermally feasible and that petrological studies currently represent the best means to determine which model is correct.

Acknowledgments

[29] We thank Peter Kelemen, Jason Phipps Morgan and two anonymous reviewers for very thorough and constructive reviews. This work was supported by the National Science Foundation under grant OCE-9629425.

References

Anderko, A., and K. S. Pitzer, Equation-of-state representation of phase equilibria and volumetric properties of the system NaCl-H_20 above 573 K, *Geochim. Cosmochim. Acta.*, *57*, 1657–1680, 1993.

Bischoff, J. L., and R. J. Rosenbauer, An empirical equation of state for hydrothermal seawater (3.2 percent NaCl), *Am. J. Sci.*, *285*, 725–763, 1985.

Bischoff, J. L., and R. J. Rosenbauer, Salinity variations in submarine hydrothermal systems by layered double-diffusive convection, *J. Geol.*, *97*, 613–623, 1989.

Boudier, F., A. Nicolas, and B. Ildefonse, Magma chambers in the Oman ophiolite: Fed from the top and the bottom, *Earth Planet. Sci. Lett.*, *144*, 239–250, 1996.

Chen, Y. J., Thermal effects of gabbro accretion from a deeper second melt lens at the fast spreading East Pacific Rise, *J. Geophys. Res.*, *106*, 8581–8588, 2001.

Chenevez, J., P. Machatel, and A. Nicolas, Numerical models of magma chambers in the Oman ophiolite, *J. Geophys. Res.*, *103*, 15,443–15,455, 1998.

Cherkaoui, A. S. M., and W. S. D. Wilcock, Characteristics of high Rayleigh number two-dimensional convection in an open-top porous layer heated from below, *J. Fluid Mech.*, *394*, 241–260, 1999.

Cherkaoui, A. S. M., and W. S. D. Wilcock, Laboratory studies of high Rayleigh number circulation in an open-top Hele-Shaw cell: An analog to mid-ocean ridge hydrothermal systems, *J. Geophys. Res.*, *106*, 10,983–11,000, 2001.

Cherkaoui, A. S. M., W. S. D. Wilcock, and E. T. Baker, Thermal fluxes associated with the 1993 diking event on the CoAxial segment, Juan de Fuca Ridge: A model for the convective cooling of a dike, *J. Geophys. Res.*, *102*, 24,887–24,902, 1997.

Clauser, C., and E. Huenges, Thermal conductivity of rocks and minerals, in *Rock Physics and Phase Relations: A Handbook of Physical Constants*, *AGU Ref. Shelf Ser.*, vol. 3, edited by T. Ahrens, pp. 105–126, AGU, Washington, D.C., 1995.

Coogan, L. A., K. M. Gillis, C. J. MacLeod, G. M. Thompson, and R. Hékinian, Petrology and geochemistry of the lower ocean crust formed at the East Pacific Rise and exposed at Hess Deep: A synthesis and new results, *Geochem. Geophys. Geosyst.*, *3*(11), 8604, doi:10.1029/2001GC000230, 2002.

Crawford, W. C., and S. C. Webb, Variations in the distribution of magma in the lower crust and at the Moho beneath the East Pacific Rise at 9°–10°N, *Earth Planet. Sci. Lett.*, *203*, 117–130, 2002.

Delaney, J. R., D. S. Kelley, M. D. Lilley, D. A. Butterfield, J. A. Baross, W. S. D. Wilcock, R. W. Embley, and M. Summit, The quantum event of oceanic crustal accretion: Impacts of diking at mid-ocean ridges, *Science*, *281*, 222–230, 1998.

Detrick, R. S., P. Buhl, E. Vera, J. Mutter, J. Orcutt, J. Madsen, and T. Brocher, Multi-channel seismic imaging of a crustal magma chamber along the East Pacific Rise, *Nature*, *326*, 35–41, 1987.

Dunn, R. A., D. R. Toomey, and S. C. Solomon, Three-dimensional seismic structure and physical properties of the crust

and shallow mantle beneath the East Pacific Rise at 9°30′N, *J. Geophys. Res.*, *105*, 23,537–23,555, 2000.

Fisher, A. T., Permeability within basaltic oceanic crust, *Rev. Geophys.*, *36*, 143–182, 1998.

Fisher, A. T., and K. Becker, Channelized fluid flow in oceanic crust reconciles heat-flow and permeability data, *Nature*, *403*, 71–74, 2000.

Garrido, C. J., P. B. Kelemen, and G. Hirth, Variation of cooling rate with depth in lower crust formed at an oceanic spreading ridge: Plagioclase crystal size distributions in Gabbros from the Oman ophiolite, *Geochem. Geophys. Geosyst.*, *2*, Paper number 2000GC000136, 2001.

Ghiorso, M. S., Thermodynamic models of igneous processes, *Annu. Rev. Earth Planet. Sci.*, *25*, 221–241, 1997.

Gill, A. E., A proof that convection in a porous vertical slab is stable, *J. Fluid Mech.*, *35*, 545–547, 1969.

Gregory, R. T., and H. P. Taylor, An oxygen isotope profile in a section of Cretaceous oceanic crust, Samail ophiolite, Oman: Evidence for $D^{18}O$ buffering of oceans by deep (>5 km) seawater-hydrothermal circulation at mid-ocean ridges, *J. Geophys. Res.*, *86*, 2737–2755, 1981.

Haymon, R. M., D. J. Fornari, M. H. Edwards, S. Carbotte, D. Wright, and K. C. Macdonald, Hydrothermal vent distribution along the East Pacific Rise crest (9°09′–54′N) and its relationship to magmatic and tectonic processes on fast-spreading mid-ocean ridges, *Earth Planet. Sci. Lett.*, *104*, 513–534, 1991.

Henstock, T. J., A. W. Woods, and R. S. White, The accretion of oceanic crust by episodic sill intrusion, *J. Geophys. Res.*, *98*, 4143–4161, 1993.

Jupp, T., and A. Schultz, A thermodynamic explanation for black smoker temperatures, *Nature*, *403*, 880–883, 2000.

Kelemen, P. B., and E. Aharonov, Periodic formation of magma fractures and generation of layered gabbros in the lower crust beneath oceanic spreading ridges, in *Faulting and Magmatism at Mid-Ocean Ridges*, *Geophys. Monogr. Ser.*, vol. 106, edited by W. R. Buck et al., pp. 267–289, AGU, Washington, D.C., 1998.

Kelemen, P. B., K. Koga, and N. Shimizu, Geochemistry of gabbro sills in the crust/mantle transition zone of the Oman ophiolite: Implications for the origin of the oceanic lower crust, *Earth. Planet. Sci. Lett.*, *146*, 475–488, 1997.

Kelley, D. S., and G. Frueh-Green, Volatile lines of descent in submarine plutonic environments: Insights from stable Isotope and fluid inclusion analyses, *Geochim. Cosmochim. Acta*, *65*, 3325–3346, 2001.

Korenaga, J., and P. B. Kelemen, Melt migration through the oceanic lower crust: A constraint from melt percolation modeling with finite solid diffusion, *Earth Planet. Sci. Lett.*, *156*, 1–11, 1998.

Lécuyer, C., and B. Reynard, High temperature alteration of oceanic gabbros by seawater (Hess Deep, Ocean Drilling Program Leg 147): Evidence from oxygen isotopes and elemental fluxes, *J. Geophys. Res.*, *101*, 15,883–15,897, 1996.

Lister, C. R. B., Heat transfer between magmas and hydrothermal systems, or, six lemmas in search of a theorem, *Geophys. J. Int.*, *120*, 45–59, 1995.

MacLeod, C. J., and G. Yaouancq, A fossil melt lens in the Oman ophiolite: Implications for magma chamber processes at fast spreading ridges, *Earth Planet. Sci. Lett.*, *176*, 357–373, 2000.

Manning, C. E., and C. J. MacLeod, Fracture-controlled metamorphism of Hess Deep gabbros, site 894: Constraints on the root zones of mid-ocean ridge hydrothermal systems at fast spreading centers, *Proc. Ocean Drill. Program Sci. Res.*, *147*, 189–212, 1996.

Manning, C., P. E. Weston, and K. I. Mahon, Rapid high temperature metamorphism of the East Pacific Rise gabbros from Hess Deep, *Earth Planet. Sci. Lett.*, *144*, 123–132, 1996.

Manning, C. E., C. J. MacLeod, and P. E. Weston, Lower crustal cracking front at fast-spreading ridges: Evidence from the East Pacific Rise and Oman ophiolite, in *Ophiolites and Oceanic Crust: New Insights from Field Studies and the Ocean Drilling Program*, edited by Y. Dilek et al., *Spec. Pap. Geol. Soc. Am.*, *349*, 261–272, 2001.

McCollom, T. M., and E. L. Shock, Fluid-rock interactions in the lower oceanic crust: Thermodynamic models of hydrothermal alteration, *J. Geophys. Res.*, *103*, 547–575, 1998.

Meyer, C. A., R. B. McClintock, G. J. Silvestri, and R. C. Spencer Jr., *ASME Steam Tables: Thermodynamic and Transport Properties of Steam*, 436 pp., Am. Soc. of Mech. Eng., New York, 1993.

Morton, J. L., and N. H. Sleep, A mid-ocean ridge thermal model: Constraints on the volume of axial hydrothermal heat flux, *J. Geophys. Res.*, *90*, 11,345–11,353, 1985.

Mottl, M. J., Hydrothermal processes at seafloor spreading centers: Application of basalt-seawater experimental results, in *Hydrothermal Processes at Seafloor Spreading Centers*, edited by P. A. Rona et al., pp. 199–224, Plenum Press, New York, 1983.

Nicolas, A., Kinematics in magmatic rocks with special reference to gabbros, *J. Petrol.*, *33*, 891–915, 1992.

Nicolas, A., and B. Ildefonse, Flow mechanism and viscosity in basaltic magma chambers, *Geophys. Res. Lett.*, *23*, 2013–2016, 1996.

Nicolas, A., I. Reuber, and K. Benn, A new magma chamber model based on structural studies in the Oman ophiolite, *Tectonophys*, *151*, 87–105, 1988.

Nicolas, A., C. Freydier, M. Godard, and A. Vauchez, Magma chambers at mid-ocean ridges: How large?, *Geology*, *21*, 53–56, 1993.

Pallister, J. S., and C. A. Hopson, Samail ophiolite plutonic suite: Field relations, phase variation, cryptic variation and layering, and a model of a spreading ridge magma chamber, *J. Geophys. Res.*, *86*, 2593–2644, 1981.

Patankar, S. V., *Numerical Heat Transfer and Fluid Flow*, 153 pp., Hemisphere, Washington, D.C., 1980.

Phipps Morgan, J., and Y. J. Chen, The genesis of oceanic crust: Magma injection, hydrothermal circulation, and crustal flow, *J. Geophys. Res.*, *98*, 6283–6297, 1993.

Phipps Morgan, J., A. Harding, J. Orcutt, G. Kent, and Y. J. Chen, An observational and theoretical synthesis of magma chamber geometry and crustal genesis along a mid-ocean

ridge spreading center, in *Magmatic Systems*, edited by M. P. Ryan, pp. 139–178, Academic, San Diego, Calif., 1994.

Pitzer, K. S., J. C. Peiper, and R. H. Busey, Thermodynamic properties of aqueous sodium chloride solutions, *J. Phys. Chem. Ref. Data*, *13*, 1–106, 1984.

Quick, J. E., and R. P. Denlinger, Ductile deformation and the origin of layered gabbro in ophiolites, *J. Geophys. Res.*, *98*, 14,015–14,027, 1993.

Rabinowicz, M., J.-C. Sempéré, and P. Genthon, Thermal convection in a vertical permeable slot: Implications for hydrothermal circulation along mid-ocean ridges, *J. Geophys. Res.*, *104*, 29,275–29,292, 1999.

Schouten, H., and C. Denham, Virtual ocean crust (abstract), *EOS Trans. AGU*, *76*(17), Spring Meet. Suppl., S48, 1995.

Sinton, J. M., and R. S. Detrick, Mid-ocean ridge magma chambers, *J. Geophys. Res.*, *97*, 197–216, 1992.

Sleep, N. H., Formation of oceanic crust: Some thermal constraints, *J. Geophys. Res.*, *80*, 4037–4042, 1975.

Wilcock, W. S. D., Cellular convection models of mid-ocean ridge hydrothermal circulation and the temperatures of black smoker fluids, *J. Geophys. Res.*, *103*, 2585–2596, 1998.

Wilcock, W. S. D., and J. R. Delaney, Mid-ocean ridge sulfide deposits: Evidence for heat extraction from magma chambers or cracking fronts?, *Earth Planet. Sci. Lett.*, *149*, 49–64, 1997.

Wilcock, W. S. D., S. C. Solomon, G. M. Purdy, and D. R. Toomey, The seismic attenuation structure of a fast-spreading mid-ocean ridge, *Science*, *258*, 1470–1474, 1992.